Reaction Kinetics, Mechanisms and Catalysis (2023) 136:449–463
https://doi.org/10.1007/s11144-022-02330-7

Conversion of heavy metal adsorbents into catalysts for the degradation of rhodamine B by high temperature activation

Jiaqi Wang[1] · Tiexin Cheng[1] · Guangdong Zhou[1]

Received: 13 October 2022 / Accepted: 11 November 2022 / Published online: 16 November 2022

Abstract
In this work, calcium nitrate and sodium silicate were employed as the sources of calcium and silicon, respectively, to synthesize sheet calcium silicate hydrate (CSH) by simple chemical precipitation. The obtained sheet CSH exhibited fast adsorption rate and large adsorption capacity, the maximum adsorption capacity is 556.3 mg g^{-1}, for Cu(II) ions. The CSH after adsorption of Cu(II) ions (CSH-Cu) was characterized by XRD, FTIR, SEM, N_2 adsorption and XPS, and which could be converted into a catalyst for rhodamine B (RhB) degradation by a simple high-temperature activation process. The results showed that the catalyst give the excellent reusability, and after four cycles of the catalyst, more than 90% of the RhB could still be degraded within 240 min. The free radical trapping experiments showed that all of the ·OH, $\cdot O_2^-$ and h^+ generated on the surface of the catalyst played an essential role in the degradation process, while h^+ made the largest contribution. Based on this, the degradation mechanism of RhB is also proposed.

Keywords Adsorption · Calcium silicate hydrate · Cu(II) ions · Degradation · Reusability · Rhodamine B

Introduction

Urbanization, industrialization, rapid population growth and misuse of water resources have led to severe water pollution. Fresh water is essential for almost all life on earth. However, the textile, coating, electroplating and other industries produce large amounts of effluent during industrial processes. For example: nickel, silver, chromium and cadmium are widely used in the electroplating industry for steel coating; in the painting

✉ Guangdong Zhou
zhougd@jlu.edu.cn

[1] College of Chemistry, Jilin University, Changchun 130012, Jilin Province, China

industry, paint has mercury and lead; methylene blue (MB), acid orange 7 (AO7) and rhodamine B (RhB) are three typical organic dyes in the textile industry.

Heavy metals can bioaccumulate and eventually enter the human body. At present, there are many methods being used to treat heavy metal ions in water, among which the adsorption is considered one of the most suitable and effective methods. Researchers have made great efforts to prepare adsorbents with excellent adsorption capacity. However, there are significant challenges in the disposal of adsorbents after adsorption of heavy metal ions. Common disposal methods for waste sorbents include desorption, incineration and landfill, all of which can cause secondary pollution or consume excessive energy [1]. In recent years, various researchers have been investigating how to transform heavy metal ion adsorbents into valuable materials. They have obtained excellent photocatalysts for hydrogen evolution in water electrolysis by converting waste adsorbates after the removal of heavy metal ions into corresponding metal sulfides by in-situ sulfide treatment [2, 3].

CSH is the main product of Portland cement hydration and has several advantages. The first is its abundance and low production costs. Second, it has great thermal stability and is suitable as a catalyst support [4]. In addition, it has a high ion exchange capacity for the rapid removal of heavy metal ions and an elevated adsorption capacity [5]. CSH also has a large number of hydroxyl groups on its surface [6], which contributes to remove heavy metals. Therefore, CSH can be used as a suitable adsorbent to removing heavy metal ions. Copper-based catalysts have been the focus of numerous studies due to their high abundance, low cost, strong solubility, low secondary contamination, and significant reactivity to hydrogen peroxide. Both Cu^{2+} and Cu^{+} can react with H_2O_2 to produce reactive radicals. The reaction of Cu^{2+} with H_2O_2 converts Cu^{2+} to Cu^{+}, and the reaction of Cu^{+} with H_2O_2 converts Cu^{+} to Cu^{2+}. Cu^{2+}/Cu^{+} is prone to cyclic reactions, which can accelerate interfacial electron transfer and improve the catalytic efficiency [7]. In addition, Cu ions can exhibit reactivity to H_2O_2 over a wide pH range, which allows H_2O_2 to efficiently generate reactive radicals that can degrade organic pollutants and achieve complete mineralization.

In this work, calcium nitrate and sodium silicate were used as sources of calcium and silicon, respectively, and cetyltrimethylammonium bromide was used as a template agent for the synthesis of CSH with a sheet structure. CSH was used to adsorb heavy metal Cu(II) ions from aqueous solutions. Subsequently, it was converted into an efficient catalyst for the degradation of RhB by a simple thermal treatment. The effect of different physical and chemical conditions on the degradation of RhB has been investigated and the reaction mechanism of RhB was degradation has been explored. The waste adsorbent was converted into a catalyst by simple thermal treatment, which not only solved the disposal problem of waste adsorbent, but also provided a catalyst for the degradation of organic pollutants, transforming waste into treasure, which meets the requirements of sustainable development.

Experimental section

Materials

Cetyltrimethylammonium bromide (99.0%, China Huishi Biochemical Reagent Factory), $Ca(NO_3)_2{\cdot}4H_2O$ (99.0%, Tianjin Guangfu Fine Chemical Research Institute), $Na_2SiO_3{\cdot}9H_2O$ (Xilong Chemical Plant), $Cu(NO_3)_2{\cdot}3H_2O$ (99.5%, Tianjin Fuchen Chemical Reagent Factory), Sodium diethyl dithiocarbamate (Shanghai Reagent No.3 Factory), rhodamine B (99.0%, Guangzhou Chemical Reagent Factory), tert-butanol (Tianjin Huadong Reagent Factory), Ammonium oxalate (99.8%, Tianjin Guangfu Technology Development Co. LTD), p-benzoquinone (Maclean), ethylene diamine tetraacetic acid disodium (99.0%, Aladdin), $NH_3{\cdot}H_2O$ (25.0%), HCl (36.0–38.0%), NaOH (96.0%) and H_2O_2 (30.0%) were purchased from Beijing Chemical Factory. All of the above reagents are analytically pure without additional treatment. All solutions were prepared with deionized water.

Preparation of CSH

Calcium silicate hydrate was synthesized by a chemical precipitation method as follows [8]. 1.4168 g $Ca(NO_3)_2{\cdot}4H_2O$ was dissolved in 80 mL deionized water and stirred for 1 h at room temperature to completely dissolve it. 0.0656 g cetyltrimethylammonium bromide (3%) was added to it. The water bath was heated to 45 °C and stirred for 1 h to gradually form a white gel. Then 40 mL 0.15 M $Na_2SiO_3{\cdot}9H_2O$ was slowly dropped into the mixture, and stirred continuously at 45 °C for 5 h. The mixture was then aged at room temperature for 24 h. After centrifugation at 8000 r/min, the mixture was washed three times with deionized water and ethanol. Finally, the samples were dried in a vacuum oven at 40 °C for 12 h and stored in a vacuum desiccator for subsequent experiments.

Characterization

The phase composition of the powders was analyzed in the range of 10–70° using an Empyrean X-ray diffractometer (XRD) with Cu K_α radiation at a voltage of 40 kV and a current of 40 mA. The chemical bonds of CSH were evaluated by a Nicolet IS5 FT-IR spectrometer in the scan range of 400–4000 cm^{-1}. The morphology of the samples was observed with SU8020 cold field emission scanning electron microscope (SEM), and the element distribution on the sample surface was tested with Bruker energy spectrometer. The elemental composition and valence state of the sample surface were evaluated with X-ray photoelectron spectroscopy (Thermo ESCA LAB 250). N_2 adsorption–desorption tests were performed by a specific surface area analyzer (Micromeritics AS 2010). The concentration of copper ions was measured at a wavelength of 452 nm using a UV-1700 spectrophotometer, and the absorbance of RhB was measured at a wavelength of 554 nm.

Copper ion adsorption experiment

The adsorption of Cu(II) ions by CSH under distinct conditions was investigated by batch adsorption experiments. $Cu(NO_3)_2{\cdot}3H_2O$ was used as the source of heavy metal ions. The pH of the solution was adjusted using 0.1 mol L^{-1} of HCl and 0.1 mol L^{-1} of NaOH solution. 3 mL of the suspension was taken at different time intervals, filtered through a 0.22 μm filter, and then tested at a wavelength of 452 nm according to the method of Sun et al. [9]. All adsorption experiments were performed in three parallel runs to observe the reproducibility of the results. The calculation formulas for the removal rate and adsorption capacity (Q_t) of Cu(II) ions are as follows:

$$\text{Removal efficiency}(\%) = \frac{C_0 - C_t}{C_0} \times 100\% \tag{1}$$

$$Q_t = \frac{C_0 - C_t}{m} \times V \tag{2}$$

Here, C_0 and C_t are concentrations of Cu(II) ions at initial time and at the time of sampling (mg/L). V (L) is the solution volume and m (g) is the Mass of adsorbent.

Reusability experiment

CSH dissolves under acidic conditions [10], so CSH after adsorption of Cu(II) ions cannot be re-adsorbed by desorption. To solve this issue, we proposed a simple method to convert CSH-Cu into a catalyst for degrading RhB by simple thermal treatment. The CSH-Cu was heated to 300 °C for 2 h to obtain catalysts CSH-Cu (300 °C), which was cooled to room temperature and stored for backup. The thermally activated CSH-Cu (300 °C) was used for the degradation of RhB.

Catalytic degradation experiment of RhB by CSH-Cu(300℃)

The degradation of RhB by CSH-Cu (300 °C) and H_2O_2 was investigated under different conditions. The catalyst powder was removed by taking 3 mL of the solution at different intervals under magnetic stirring and centrifuged at 3000 r/min for 3 min. The supernatant was tested with UV–vis spectrophotometer at 554 nm wavelength to evaluate the degradation performance of RhB by CSH-Cu (300 °C). Three parallel experiments were performed for all degradation experiments.

Results and discussion

Characterization of CSH

Fig. 1a shows the X-ray diffraction pattern of the synthesized CSH. The diffraction peaks at 2θ = 29.3°, 32.0° and 50.0° are consistent with the standard JCPDS card 33-0306, indicating that the synthesized product is CSH [11]. At the same time, in the XRD pattern, it can be found that there are minor diffraction peaks at 2θ = 16.8° and 55.3°, which are Na_2SiO_3 and $Ca(NO_3)_2$, respectively. This may be due to the fact that Na_2SiO_3 and $Ca(NO_3)_2$ have not been fully reacted, and still have some residues. Fig. 1b is the FT-IR spectra of the synthesized CSH. According to the literature [12, 13], it is known that the absorption peaks in CSH can be assigned as follows: the absorption peaks at 3450 and 1641 cm^{-1} correspond to ν(O–H) and δ(O–H), respectively, which are the stretching vibration peak of bound water in CSH and the bending vibration peak of -OH group bound in water. The absorption peaks at 1400–1500 and 873 cm^{-1} are the asymmetric stretching and out-of-plane bending vibrational peaks of CO_3^{2-}, caused by the sample exposure to air. The absorption peaks at 971, 664 and 454 cm^{-1} are assigned to $\nu(Si–O)Q^2$ stretching vibration, ν_s(Si–O-Si) symmetrical stretching vibration and δ(Si–O-Si) bending vibration. The FT-IR spectra again prove that the synthesized sample is CSH, and the $[SiO_4]^{4-}$ tetrahedral structure in CSH existed in the form of Q^2.

The morphology of CSH can be observed by SEM images, as shown in Fig. 2a, the synthesized CSH consists of many interdigitated sheets forming a flower-like morphology. Fig. 2b shows the element mapping of CSH. Figures show that the CSH is composed of three elements, namely Ca, Si and O, which are uniformly dispersed.

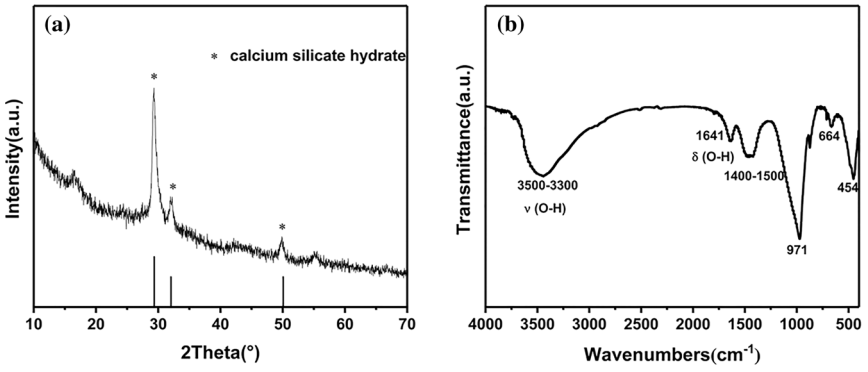

Fig. 1 **a** XRD pattern and **b** FTIR spectra of CSH

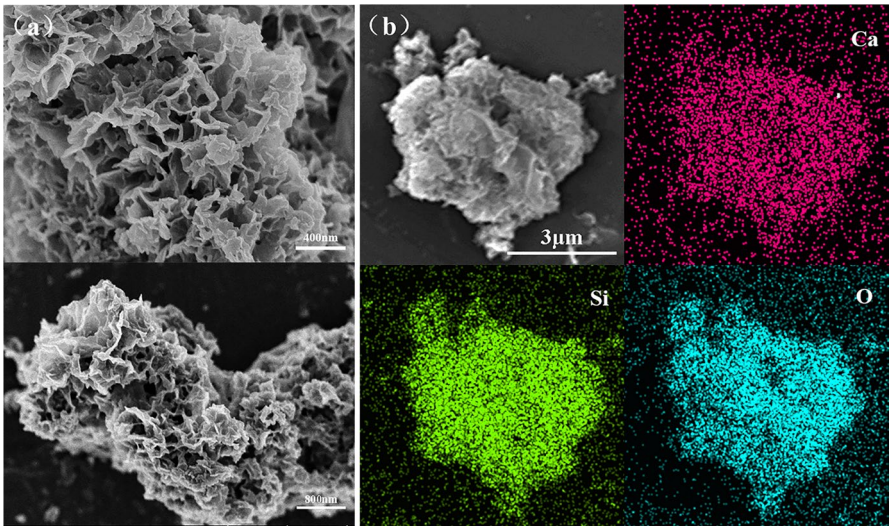

Fig. 2 **a** SEM images and **b** EDX-mapping images of CSH

Adsorption experiments of copper ions

Batch adsorption experiment

The effect of different conditions on the adsorption of Cu(II) ions was investigated. It can be seen from Fig. S1 that with the increase of adsorbent concentration, the removal efficiency of Cu(II) ions increased. This is due to an increase in the concentration of adsorbates, the number of active sites available for adsorption, and thus the removal efficiency. As shown in Fig. S2, when the initial concentration of Cu(II) ions was 200 mg/L, the amount of Cu(II) ions adsorbed within 20 min was 556.3 ± 2.4 mg/g. There are only a limited number of adsorption sites that adsorbates can provide. When the initial concentration of Cu(II) ions increases, CSH is not sufficient to provide sufficient adsorption sites, and the adsorption capacity has reached saturation. At the same time, there will be Cu(II) ions adsorbed on the surface of CSH, which hinders the adsorption. When the pH value increases from 4 to 7 (Fig. S3), both the adsorption capacity and the removal rate gradually increase, which were related to the hydroxyl groups on the surface of the adsorbent CSH. The pH of the solution should not be too high, otherwise Cu^{2+} ions will react with OH^- to form $Cu(OH)_2$ precipitation. Fig. S4 shows the effect of temperature on adsorption. The adsorption capacity and removal efficiency gradually increase with increasing temperature, indicating that the adsorption process is endothermic. As the temperature increases, the molecular motion and collision probability increases, which leads to an increase in the adsorption rate.

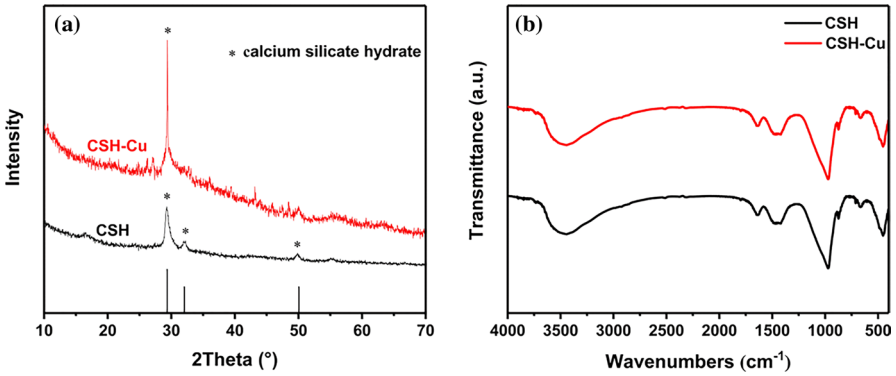

Fig. 3 **a** XRD pattern and **b** FTIR spectra of CSH before and after adsorption of Cu(II) ions

Fig. 4 SEM image of CSH-Cu

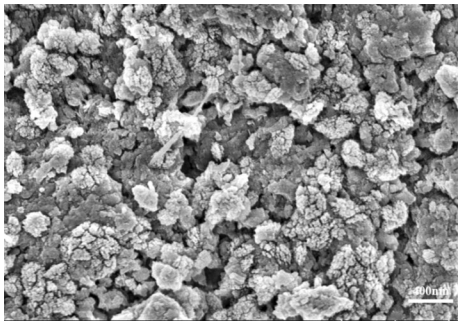

Adsorption mechanism

The XRD pattern of CSH-Cu is shown in Fig. 3a, and there is no new obvious crystal diffraction peak on the surface, indicating that Cu(II) ions are amorphous on the surface of CSH. The FT-IR spectrum (Fig. 3b) does not change significantly before and after adsorption. The SEM image of CSH-Cu is shown in Fig. 4. The obvious aggregation of CSH occurs after adsorbing Cu(II) ions. The morphology of the CSH changes from sheet to granular morphology. Figs. S5a and b show that the N_2 sorption desorption isotherms of CSH and CSH-Cu, respectively. CSH has a large specific surface area (632.2 $m^2 \cdot g^{-1}$), which is favorable for the adsorption of metal ions. After adsorbing Cu(II) ions, the specific surface area of CSH-Cu becomes 244.9 $m^2 \cdot g^{-1}$. The decrease in specific surface area was attributed to the apparent agglomeration of CSH during the adsorption process. According to the BJH method, the average pore sizes of CSH and CSH-Cu are 3.826 nm and 3.829 nm, respectively, without significant change.

The elemental binding state after the adsorption of Cu(II) ions on the surface of the adsorbent CSH can be studied by XPS. Fig. 5a shows the XPS spectra of CSH before and after Cu(II) ions adsorbing. Compared to CSH, the XPS spectra of CSH-Cu changes significantly. The peak of Cu 2p appears, while the peaks of

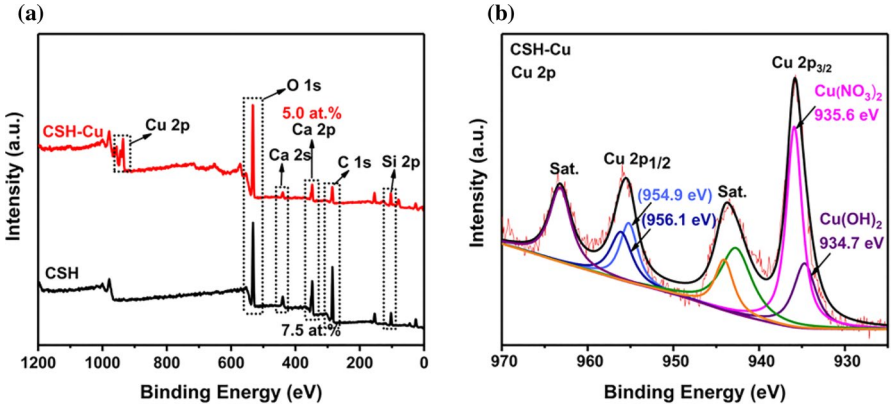

Fig. 5 XPS spectra of **a** survey scan and **b** high resolution scan of Cu 2p of CSH-Cu

Ca 2p and Ca 2s gradually decreased, which again proves the loading of Cu(II) ions and the leaching of Ca(II) ions.

To further investigate the binding state of heavy metal Cu(II) ions on the adsorbent surface, a further XPS scanning was performed on CSH-Cu, and the high-resolution XPS spectrum of Cu 2p is shown in Fig. 5b. The two signal peaks at the binding energies of 934.7 eV and 954.9 eV correspond to Cu $2p_{3/2}$ and Cu $2p_{1/2}$. The binding energies of the peak signal of the shaking satellite for Cu $2p_{3/2}$ and Cu $2p_{1/2}$ are approximately 942.7 eV and 962.6 eV, respectively. The deconvolution peaks of Cu $2p_{3/2}$ and Cu $2p_{1/2}$ at 934.7 eV and 954.9 eV, respectively, are the same as those of $Cu(OH)_2$, indicating the presence of $Cu(OH)_2$. During the adsorption process, part of the Cu^{2+} is associated with the leached OH^- and combines to form $Cu(OH)_2$ precipitates. The deconvolution peaks of Cu $2p_{3/2}$ and Cu $2p_{1/2}$ at 935.6 eV and 956.1 eV [14], respectively, indicate the presence of $Cu(NO_3)_2$ on the surface of the adsorbent, since part of the Cu^{2+} is adsorbed on the CSH surface as $Cu(NO_3)_2$. The binding energies of Cu^0 and Cu^+ signals in the Cu 2p XPS spectra are generally less than 933 eV [15], which are not observed in the spectra.

In low pH solutions, CSH is unstable and will release Ca^{2+} and OH^-. According to the study [16], CSH first released Ca^{2+} and OH^-, and then adsorbed fluoride. This unstable chemistry is considered as a drawback of CSH applications in various fields [17]. During the experiment (the initial pH was 5), not only the adsorption amount of Cu(II) ions by CSH was recorded, but also the pH value and Ca^{2+} concentration of the solution after adsorption (Fig. S6). The pH of the solution increases after the adsorption reaction. With the increase of the initial concentration of Cu(II) ions, the pH value of the solution decreased rapidly to 6.92 ± 0.03, and the adsorption capacity also reached equilibrium. The leaching of Ca^{2+} was detected in the adsorbed solution, with concentrations in the lower range of 20–30 mg/L, and no contamination to the environment. These results show that CSH releases Ca^{2+} and OH^- in the process of adsorbing Cu(II) ions. Cu^{2+} will combine with OH^- released from CSH to form $Cu(OH)_2$.

Based on the above analysis, it can be assumed that CSH removes Cu(II) ions in two ways. One way is to adsorb Cu(II) ions on the surface of CSH by physical adsorption. The other way is that Cu(II) ions combines with the OH^- released by CSH to form $Cu(OH)_2$.

Reusability experiment

CSH is unstable under acidic conditions and can release Ca^{2+} and OH^- during adsorption, so desorption and resorption methods for CSH are infeasible. Therefore, we recovered CSH-Cu (adsorption conditions: 10 mg CSH, 100 mg/L $Cu(NO_3)_2$ solution, adsorption time 30 min, adsorption capacity 408.7 ± 2.0 mg/g). After washing with deionized water, the samples were dried in a vacuum oven at 40 °C for 12 h. CSH-Cu was activated at high temperature to convert it into photocatalyst for RhB degradation.

Degradation of RhB by CSH-Cu

Five control experiments were conducted to verify the degradation properties of RhB by different reaction systems. As shown in Fig. S7, when the reaction system was: (1) only H_2O_2, (2) only CSH, (3) both CSH and H_2O_2 simultaneously, the removal rate of RhB under these three reaction systems was approximately zero. When only CSH-Cu was present in the reaction system, the removal rate of RhB was $17.9 \pm 0.3\%$ within 180 min, which was likely due to the adsorption of RhB by CSH-Cu. When both CSH-Cu and H_2O_2 were present in the reaction system, at the same time the removal rate of RhB was as high as $92.3 \pm 0.1\%$ within 180 min, which indicated that CSH-Cu could catalyze H_2O_2 to generate ·OH and $\cdot O_2^-$, which was beneficial to the degradation of RhB.

The activation temperature of CSH-Cu had an effect on the degradation of RhB. As shown in Fig. S8, with the increase in activation temperature, the removal efficiency of RhB gradually increased. When the activation temperature was greater than 300 °C, the removal efficiency gradually decreased. This may be due to the increase in the activation temperature, the removal of interlayer water from CSH and the change of the chain structure of CSH [18], which increases the specific surface area of CSH. As a result, there are more active sites on the catalyst surface, which facilitates to the degradation of RhB. However, with further increase in temperature, the CSH sheets were overlapped, reducing the specific surface area and thus the performance. Therefore, CSH-Cu with an activation temperature of 300 °C was selected for subsequent experiments.

The H_2O_2 content is one of the key parameters that influence the degradation performance of RhB. Fig. S9 is the degradation curve of RhB with different contents of H_2O_2. The H_2O_2 content was increased and the catalytic efficiency of RhB was significantly improved. This was because the higher the H_2O_2 content, the more reactive oxygen radicals could be produced and therefore the faster the rate of RhB degradation.

The effect of catalyst dosage on RhB degradation is particularly obvious (Fig. S10). The removal of RhB by CSH-Cu(300 °C) manifested in two aspects, namely

the adsorption and catalytic degradation of RhB by CSH-Cu(300 °C). When the amount of catalyst increased, the active sites on the surface of CSH-Cu (300 °C) increased which could not only adsorb more RhB, but also generate more active species for RhB degradation.

Fig. S11 shows the effect of the initial concentration of RhB on the degradation rate. The degradation rate was inversely proportional to the initial concentration of the pollutant. There were three main reasons for this. First, the initial concentration of pollutants increased, and the number of dye molecules produced increased. However, the concentration of the catalyst was fixed and the amount of RhB that could be adsorbed was limited. Second, the active sites on the catalyst surface were certain, and only a quantitative amount of active substances could be generated to degrade RhB within a certain time. In addition, there was competitive adsorption between RhB and H_2O_2 at the active site of the catalyst surface, and a large initial concentration of the dye will hinder the adsorption and catalytic decomposition of H_2O_2 at the catalyst surface [19, 20].

As shown in Fig. S12a, it is obvious that the accelerated removal efficiency is due to the increased temperature and faster molecular movement, which allow for more active substances and promotes the degradation of RhB. The degradation of RhB at different temperatures followed pseudo-first-order reaction kinetics (Fig. S12b). According to Lente's method [21, 22], the least squares fitting was performed to the pseudo-first-order kinetic exponential curve:

$$A = X * \exp(-kt) + E \tag{3}$$

Here A is the concentration of RhB dye taken from the relative concentration C/C_0, k is the pseudo-first-order rate constant (min^{-1}), X is the amplitude of the process, E is the endpoint. Using Prof. Gábor Lente at http://lenteg.ttk.pte.hu/KinetFit.html provides the Excel file to calculate the relevant data. Table 1 lists the pseudo-first-order rate constants at different temperatures. In addition, the standard deviation of parameter k and the linear correlation coefficient R^2 are also listed in the table.

The initial pH of the solution plays a key role in the catalytic reaction. Fig. S13a shows the degradation process at different initial pH. The higher initial pH of the solution is, the more effective the degradation of RhB is. This could be attributed to that the oxidation of H_2O_2 to $HO_2 \cdot$ or $\cdot O_2^-$ by Cu^{2+} was more favorable at higher pH, and the amount of more active deprotonated hydrogen peroxide (HO_2^-) increased significantly [23], which accelerated the degradation rate of RhB.

Table 1 The pseudo-first-order kinetic constants (k) of the degradation of RhB at different temperatures. (0.1 g/L catalyst and 50 μL H_2O_2)

Temperature	293.15 K	303.15 K	313.15 K	323.15 K	333.15 K
k (min^{-1})	0.0336	0.0288	0.0349	0.0863	0.1623
Standard deviation	0.0135	0.0070	0.0053	0.0067	0.0042
R^2	0.9762	0.9934	0.9963	0.9957	0.9991

Meanwhile, the dissociation of Cu^{2+} at different pH was recorded (Fig. S13b). When the pH was 2.5, the dissolution rate of total copper ions was the highest, which was 0.384 ± 0.001 mmol/L. At a pH of 10.5, the dissolution rate of the total copper ions was 0.026 ± 0.004 mmol/L and the copper ions hardly leach. Since excess Cu(II) ions could act as a radical scavenger and reduce the concentration of active species [24], it was again demonstrated that the degradation of RhB was favored at higher pH.

Reusability and stability of CSH-Cu (300 °C)

Figs. S14a–c show the sample color, XRD, FT-IR of the catalyst before and after the reaction. The color of the catalyst changed from green before the reaction to purple, which was the color of RhB after CSH-Cu (300 °C) adsorbed a part of RhB. The XRD pattern and FT-IR pattern show no obvious change in CSH-Cu (300 °C) before and after the surface reaction.

The catalyst powder after each experiment was centrifuged, washed with deionized water, dried in an ordinary oven, and then the experiment was repeated to test the reusability of CSH-Cu (300 °C). It can be seen from Fig. S14d that the removal efficiency of RhB by CSH-Cu (300 °C) decreases with the increase in the number of repetitions. After four cycles of experiments, the removal efficiency of RhB dropped to $78.3 \pm 0.4\%$ within 150 min. This could be explained by the fact that in each degradation experiment, CSH-Cu (300 °C) adsorbed a part of RhB and its intermediates in the degradation process, which could not be removed by simple washing. Since it will occupy the active sites of CSH-Cu (300 °C) and hinder the generation of active substances, the removal performance of RhB will be reduced. However, with the extension of time, more than 90% of RhB could still be removed within 240 min, and CSH-Cu (300 °C) has excellent reusability.

Reaction mechanism of RhB degradation

In order to understand the dominant active species during RhB degradation, different types of radical scavengers were added to the reaction system during degradation (Fig. S15). In this experiment, tert-butanol (IPA), p-benzoquinone (BQ) and ammonium oxalate (AO) were selected as quenchers for ·OH, $\cdot O_2^-$ and h^+. The removal rate of RhB could reach $97.7 \pm 0.1\%$ without adding quencher, and after adding IPA, BQ and AO, the removal efficiency of RhB decreased to $68.7 \pm 0.2\%$, $65.9 \pm 0.02\%$ and $31.7 \pm 0.09\%$, respectively. This phenomenon indicated that ·OH, $\cdot O_2^-$ and h^+ played a joint role in the degradation of RhB, and their contribution order was: $h^+ > \cdot O_2^- > \cdot OH$. RhB was barely degraded after EDTA was added to the reaction system. This was because EDTA formed a stable complex with Cu^{2+}, which prevented the reaction, and therefore Cu^{2+} was extremely critical for the degradation of RhB.

Based on the above experiments, we proposed a mechanism for the degradation of RhB by CSH-Cu (300 °C): First, when irradiated with light, E_g with energy higher than CSH-Cu (300 °C) will generate h^+, which can oxidize H_2O or OH^- generate ·OH [25, 26]. Secondly, CSH-Cu (300 °C) will release Cu^{2+}, and the free Cu^{2+} in the solution

can decompose H_2O_2 to generate ·OOH. ·OOH deprotonation produces strong oxidative radicals $\cdot O_2^-$ and Cu^{2+} are reduced to Cu^+ at the same time. Cu^+ can decompose H_2O_2 to produce ·OH. Since $\cdot O_2^-$ is the precursor of most reactive oxygen species [27], $\cdot O_2^-$ can also react with H_2O_2 to generate ·OH [28]. Finally, ·OH, $\cdot O_2^-$ and h^+ act together to convert RhB to CO_2 and H_2O. The main reaction formulas are as follows:

$$\mathrm{CSH-Cu(300\,^{\circ}C)} + \mathrm{hv} \rightarrow \mathrm{h^+ + e^-} \tag{4}$$

$$\mathrm{Cu^{2+} + H_2O_2} \rightarrow \mathrm{Cu^+ + \cdot HO_2 + H^+} \tag{5}$$

$$\mathrm{Cu^+ + H_2O_2} \rightarrow \mathrm{Cu^{2+} + \cdot OH + OH^-} \tag{6}$$

$$\mathrm{\cdot HO_2} \rightarrow \mathrm{\cdot O_2^- + H^+} \tag{7}$$

$$\mathrm{H_2O_2 + \cdot O_2^-} \rightarrow \mathrm{\cdot OH + O_2 + OH^-} \tag{8}$$

$$\mathrm{\cdot OH/\cdot O_2^-/h^+ + RhB} \rightarrow \mathrm{CO_2 + H_2O} \tag{9}$$

Fig. S16a shows the UV–vis absorption spectrum of degraded 10 mg/L RhB. As the illumination time is extended, the maximum absorption peak of RhB gradually decreases and finally drops to approximately zero. This indicates that in the process of degradation, the structure of RhB is destroyed and degraded into other substances. As can be seen from Fig. S16a, the absorption curve distribution of RhB decreases relatively uniformly with the reaction time progress. When the reaction time reaches 120 min, the maximum absorption peak of the RhB solution is around zero, indicating that RhB has been completely degraded. It can also be seen from the figure that the absorption peak did not shift during the first 30 min, which may be due to the combined effect of deethylation [29] and hydroxylation [30] during the degradation of RhB. Deethylation causes a blue shift of the absorption peak, while hydroxylation causes a red shift of the absorption peak, and the two effects cancel each other out, so the position of the absorption peak does not change substantially. When the reaction time increased, the maximum absorption peak of the RhB solution is slightly blue-shifted, which is due to the deethylation of the RhB molecule. Fig. S16b shows the UV–Vis absorption spectra before and after the degradation of 10 mg/L RhB. The inset shows the color change of RhB before and after the reaction, with the solution becoming colorless after the reaction. Figure shows that the UV–Vis absorption spectrum of RhB before degradation produces peaks at 258, 354 and 554 nm. However, no distinct peaks are observed after degradation, confirming RhB mineralization.

Conclusion

The sheet calcium silicate hydrate (CSH) was prepared with calcium nitrate and sodium silicate as the raw materials by simple chemical precipitation. CSH showed excellent performance in adsorbing Cu(II) ions. SEM photos revealed that after

adsorbing Cu(II) ions, these sheet CSH occurred aggregation clearly and resulted in a formation of the granular morphology. Therefore, the specific surface area decreased from 632.2 $m^2\ g^{-1}$ to 244.9 $m^2\ g^{-1}$. XPS results showed that Cu adsorbed on the CSH was mainly present as Cu(II). Activated CSH-Cu at high temperature was an excellent catalyst for the degradation of the organic dye RhB. It was shown that the degradation efficiency of RhB depended on the activation temperature of the catalyst, the concentration of H_2O_2, the concentration of CSH, the initial concentration of RhB, the temperature and the initial pH value of the solution. This catalyst is able to degrade RhB over a wide range of pH values. The free radical trapping experiment showed that •OH, $\bullet O_2^-$ and H^+ played a common role in the degradation of RhB, and the contribution order was $h^+ > \cdot O_2^- > \cdot OH$. At the same time, the presence of Cu(II) ions plays a key role in the degradation. The catalyst has superior reusability and can still remove more than 90% of RhB within 240 min after four cycles of the experiment. Based on the changes in the UV–vis absorption spectra during RhB degradation, it can be inferred that both deethylation and hydroxylation play a role in RhB degradation. This paper is of significant implications for the treatment of waste adsorbents and wastewater. CSH has great promise in wastewater purification.

Supplementary Information The online version contains supplementary material available at https://doi.org/10.1007/s11144-022-02330-7.

Author contributions JW: conceptualization, methodology, software, investigation, writing-original draft. TC: validation. GZ: conceptualization, methodology, resources, writing-review and editing.

Data availability This article data is available to authorized users.

Declarations

Conflict of interest The authors declare no conflict of interest requiring disclosure in this article.

References

1. Chen FF, Liang Y, Chen LN, Liang X, Feng YN, Wu J et al (2021) Upcycling of heavy metal adsorbents into sulfide semiconductors for photocatalytic CO_2 reduction. Appl Surf Sci. https://doi.org/10.1016/j.apsusc.2021.149647
2. Xu YF, Zhang C, Lu P, Zhang XH, Zhang LX, Shi JL (2017) Overcoming poisoning effects of heavy metal ions against photocatalysis for synergetic photo-hydrogen generation from wastewater. Nano Energy 38:494–503. https://doi.org/10.1016/j.nanoen.2017.06.019
3. Wang M, Yao HL, Zhang LL, Zhou XX (2020) Synthesis of highly-efficient photocatalyst for visible- light-driven hydrogen evolution by recycling of heavy metal ions in wastewater. J Hazard Mater. https://doi.org/10.1016/j.jhazmat.2019.121149
4. Sheng KF, Zeng F, Pang F, Ge JP (2019) Highly dispersed Ni nanoparticles on anhydrous calcium silicate (ACS) nanosheets for catalytic dry reforming of methane: tuning the activity by different ways of Ni introduction. Chem-Asian J 14(16):2889–2897. https://doi.org/10.1002/asia.201900611
5. Zhao J, Zhu YJ, Wu J, Zheng JQ, Zhao XY, Lu BQ et al (2014) Chitosan-coated mesoporous microspheres of calcium silicate hydrate: Environmentally friendly synthesis and application as a highly efficient adsorbent for heavy metal ions. J Colloid Interf Sci 418:208–215. https://doi.org/10.1016/j.jcis.2013.12.016
6. Shao NN, Tang SQ, Liu Z, Li L, Yan F, Liu F et al (2018) Hierarchically structured calcium silicate hydrate-based nanocomposites derived from steel slag for highly efficient heavy metal removal from

wastewater. Acs Sustain Chem Eng 6(11):14926–14935. https://doi.org/10.1021/acssuschemeng.8b03428
7. Wang LF, Liu YG, Lin YJ, Yu YH, Zhang XY, Zhang RQ et al (2021) One-step synthesis of novel Ni-doped $Cu_2(OH)_3F$ Fenton-like catalyst driven by visible light: Single activity and synergistic effect enhanced by bimetallic cooperation. J Alloy Compd. https://doi.org/10.1016/j.jallcom.2021.161424
8. Liu LH, Yang GG, Wang YF, Li T, Tang AP (2016) Synthesis of mesoporous calcium silicate by template method and its adsorption performance for heavy metal ions. Environ Chem 35(9):1943–1951
9. Sun DZ, Sun Y, Qin ZB, Gao J, Gao J (2019) Improvement of spectrophotometric method for determination of copper ions concentration in solution by copper reagent. Chem Eng. https://doi.org/10.16247/j.cnki.23-1171/tq.20190370
10. Richardson IG (2008) The calcium silicate hydrates. Cement Concrete Res 38(2):137–158. https://doi.org/10.1016/j.cemconres.2007.11.005
11. Zhang ML, Chang J (2010) Surfactant-assisted sonochemical synthesis of hollow calcium silicate hydrate (CSH) microspheres for drug delivery. Ultrason Sonochem 17(5):789–792. https://doi.org/10.1016/j.ultsonch.2010.01.012
12. Lu P, Li Q, Zhai JP (2008) Mineralogical characterizations and reaction path modeling of the pozzolanic reaction of fly ash-lime systems. J Am Ceram Soc 91(3):955–964. https://doi.org/10.1111/j.1551-2916.2007.02193.x
13. Yu P, Kirkpatrick RJ, Poe B, Mcmillan PF, Cong XD (1999) Structure of calcium silicate hydrate (C-S-H): Near-, mid-, and far-infrared spectroscopy. J Am Ceram Soc 82(3):742–748
14. Akhavan O, Azimirad R, Safa S, Hasani E (2011) $CuO/Cu(OH)_2$ hierarchical nanostructures as bactericidal photocatalysts. J Mater Chem 21(26):9634–9640. https://doi.org/10.1039/c0jm04364h
15. Lopez-Suarez FE, Bueno-Lopez A, Illan-Gomez MJ, Adamski A, Ura B, Trawczynski J (2008) Copper catalysts for soot oxidation: alumina versus perovskite supports. Environ Sci Technol 42(20):7670–7675. https://doi.org/10.1021/es8009293
16. Guan W, Zhao X (2016) Fluoride recovery using porous calcium silicate hydrates via spontaneous Ca^{2+} and OH^- release. Sep Purif Technol 165:71–77. https://doi.org/10.1016/j.seppur.2016.03.050
17. Shi C, Stegemann JA (2000) Acid corrosion resistance of different cementing materials. Cement Concrete Res 30(5):803–808. https://doi.org/10.1016/S0008-8846(00)00234-9
18. Wang Z, Li T, Zhao Q, Wang D, Cui X (2021) Adsorption of methylene blue by modified tobermorite. J Chin Ceram Soc 49(06):1185–1194. https://doi.org/10.14062/j.issn.0454-5648.20200792
19. Wang CQ, Cao YJ, Wang H (2019) Copper-based catalyst from waste printed circuit boards for effective Fenton-like discoloration of Rhodamine B at neutral pH. Chemosphere 230:278–285. https://doi.org/10.1016/j.chemosphere.2019.05.068
20. Wang DY, Zou J, Cai HH, Huang YX, Li F, Cheng QF (2019) Effective degradation of orange G and rhodamine B by alkali-activated hydrogen peroxide: roles of HO_2^- and O_2^-. Environ Sci Pollut R 26(2):1445–1454. https://doi.org/10.1007/s11356-018-3710-7
21. Lente G (2018) Facts and alternative facts in chemical kinetics: remarks about the kinetic use of activities, termolecular processes, and linearization techniques. Curr Opin Chem Eng 21:76–83. https://doi.org/10.1016/j.coche.2018.03.007
22. Lente G (2015) Deterministic kinetics in chemistry and systems biology: the dynamics of complex reaction networks. Springer, New York
23. Skounas S, Methenitis C, Pneumatikakis G, Morcellet M (2010) Kinetic studies and mechanism of hydrogen peroxide catalytic decomposition by Cu(II) complexes with polyelectrolytes derived from L-Alanine and glycylglycine. Bioinorg Chem Appl. https://doi.org/10.1155/2010/643120
24. Xin SS, Liu GC, Ma XH, Gong JX, Ma BR, Yan QH et al (2021) High efficiency heterogeneous Fenton-like catalyst biochar modified $CuFeO_2$ for the degradation of tetracycline: Economical synthesis, catalytic performance and mechanism. Appl Catal B-Environ. https://doi.org/10.1016/j.apcatb.2020.119386
25. Nie YC, Yu F, Wang LC, Xing QJ, Liu X, Pei Y et al (2018) Photocatalytic degradation of organic pollutants coupled with simultaneous photocatalytic H-2 evolution over graphene quantum dots/Mn-N-TiO_2/g-C_3N_4 composite catalysts: Performance and mechanism. Appl Catal B-Environ 227:312–321. https://doi.org/10.1016/j.apcatb.2018.01.033
26. Barrocas B, Entradas TJ, Nunes CD, Monteiro OC (2017) Titanate nanofibers sensitized with ZnS and Ag_2S nanoparticles as novel photocatalysts for phenol removal. Appl Catal B-Environ 218:709–720. https://doi.org/10.1016/j.apcatb.2017.06.089

27. Turrens JF (2003) Mitochondrial formation of reactive oxygen species. J Physiol 552(2):335–344. https://doi.org/10.1113/jphysiol.2003.049478
28. Xing ST, Zhou ZC, Ma ZC, Wu YS (2011) Characterization and reactivity of Fe_3O_4/$FeMnO_x$ core/shell nanoparticles for methylene blue discoloration with H2O2. Appl Catal B-Environ 107(3–4):386–392. https://doi.org/10.1016/j.apcatb.2011.08.002
29. Fu HB, Zhang SC, Xu TG, Zhu YF, Chen JM (2008) Photocatalytic degradation of RhB by fluorinated Bi_2WO_6 and distributions of the intermediate products. Environ Sci Technol 42(6):2085–2091. https://doi.org/10.1021/es702495w
30. Prevot AB, Basso A, Baiocchi C, Pazzi M, Marci G, Augugliaro V et al (2004) Analytical control of photocatalytic treatments: degradation of a sulfonated azo dye. Anal Bioanal Chem 378(1):214–220. https://doi.org/10.1007/s00216-003-2286-2